PAPER

Check for updates

Electrochemical properties of kenaf-based activated carbon monolith for supercapacitor electrode applications†

Han Yul Park,[a] Minhu Huang,[b] Tae-Ho Yoon [ID] *[b] and Kyung Hun Song*[a]

Activated carbon monoliths of kenaf (ACMKs) were prepared by moulding kenaf fibers into a column-shape monolith and then carrying out pyrolysis at 500, 600, 700 or 800 °C, followed by activation with KOH at 700 °C. Then, the sample was characterized using thermogravimetric analyzer (TGA), field-emission scanning electron microscopy (FE-SEM), field-emission transmission electron microscopy (FE-TEM), X-ray photoelectron spectroscopy (XPS), Raman spectroscopy, X-ray diffraction (XRD) and N_2 sorption instruments. The prepared ACMK was subjected to electrochemical property evaluation *via* cyclic voltammetry (CV), galvanostatic charge–discharge (GCD) and electrochemical impedance spectroscopy (EIS). The GCD study using a three-electrode system showed that the specific capacitance decreased with higher pyrolysis temperature (PYT) with the ACMK pyrolyzed at 500 °C (ACMK-500) exhibiting the highest specific capacitance of 217 F g^{-1}. A two-electrode system provided 95.9% retention upon a 5000 cycle test as well as the specific capacitance of 212 F g^{-1}, being converted to an energy density of 6 W h kg^{-1} at a power density of 215 W kg^{-1}.

Introduction

Activated carbons (ACs) are widely used in many areas of application, including purification of water and air, sequestration of carbon dioxide, and catalyst carriers because of their large surface area, high chemical, thermal and mechanical stability, and environmental friendliness.[1] Recently, much attention has been focused on ACs as possible electrode materials for supercapacitors since they are more advantageous than batteries in terms of faster charge–discharge, higher power density and longer life.[2]

Such broad applications of ACs have resulted in a depletion of wood, fossil and other raw materials used in the production of ACs, and a need for alternative materials such as polymers which are readily available and can produce high quality AC. However, polymers failed to gain popularity because of the complicated production process involved until Pekala introduced a simple hydrothermal polycondensation reaction of resorcinol and formaldehyde,[3] which is similar to the sol–gel process.[4]

Despite such success, the AC from resorcinol and formaldehyde had two critical drawbacks for electrode applications.

First, their powdery form generally required a binder to fabricate the electrode, along with a conductivity enhancer and a solvent to achieve better property and easier processing, respectively. Unfortunately, such additives not only increased the total weight and production cost of the electrode but also deteriorated its electrochemical performance. This led to the preparation of carbon monoliths (CMs).[5,6]

Second, the process required the use of a catalyst, template and/or a special drying process in order to afford fast reaction, form micro- and/or meso-pores or avoid pore collapsing, respectively, making the reaction complicated. Thus, a number of attempts were made to exclude such steps, but only partial success was achieved in excluding the template, as reported by Pekala[7] as well as Baumann.[8] Recently, however, the successful preparation of CM xerogels that exclude all three steps was reported with good electrochemical properties.[9,10]

Because of the high price of polymers, biomasses or biowastes have also been studied as alternatives since they are abundant, inexpensive, renewable and sustainable.[11,12] Among them, kenaf is an attractive candidate for AC production because of its low price and large annual production (2.8 million tons in 1985).[13] Kenaf was initially cultivated for its fibers to make rope and coarse twine fabric, but its use has dramatically dropped recently with the introduction of polymer-based fibers and production decreased to 300 000 tons in 2016.[14] Therefore, attempts have been made to broaden its application to the production of paper, composites, oil spill absorbents, bio-fuel and livestock bedding.[15] Unfortunately, its consumption did not increase as desired.

[a]*Department of Clothing and Textiles, Pai Chai University, 155-40 Baejae-ro (Doma-Dong), Seo-gu, Daejeon, 35345, South Korea. E-mail: khsong@pcu.ac.kr; Fax: +82-70-4850-8468; Tel: +82-42-520-5413*

[b]*School of Materials Science and Engineering, Gwangju Institute of Sci. and Tech. (GIST), 123 Cheomdangwagi-ro, Buk-gu, Gwangju, 61005, South Korea. E-mail: thyoon@gist.ac.kr; Fax: +82-62-715-2304; Tel: +82-62-715-2307*

† Electronic supplementary information (ESI) available. See DOI: 10.1039/d1ra07815a

Recently, kenaf fibers as well as kenaf stems have been used to prepare ACs for supercapacitor electrodes,[16–18] adsorption[19,20] and catalyst support.[21] However, the specific capacitance of the kenaf-based carbon was only 37 F g^{-1} (ref. 16) despite the fact that it was enhanced to 136 F g^{-1} by polyaniline coating. On the other hand, high capacitance of 416 and 327 F g^{-1} were reported with MnO_2 decorated kenaf-stem-derived 3D carbon[17] and $NiCl_2$ activated nanosheet of the kenaf stem.[18] The latter studies demonstrate the high potential of kenaf-based ACs for supercapacitor electrode applications.

As mentioned, kenaf-based ACs used in these studies were in powder form and required binders to fabricate the electrode, causing the problems discussed above. This has raised the possibility of preparing CM of the kenaf fibers, but no studies are available to date despite the successful preparation of CM reported with other bio-wastes such as oil palm empty fruit bunch fibers,[22] saw dust[23] and cellulose fibers.[24]

In this study, therefore, the preparation of CM with kenaf fibers was attempted by moulding. The powder form of kenaf fibers obtained from local-farm-grown kenaf plant was moulded into column shape samples, followed by pyrolysis and KOH activation. Their electrochemical properties were evaluated with a three-electrode system via cyclic voltammetry (CV), galvanostatic charge–discharge (GCD) and electrochemical impedance spectroscopy (EIS). A two-electrode system was also studied but only for the sample with the highest capacitance. The samples were also characterized by thermogravimetric analyser (TGA), field emission scanning electron microscopy (FE-SEM), X-ray photoelectron spectroscopy (XPS), Raman spectroscopy, X-ray diffraction (XRD), and N_2 sorption instrument.

Experimental

Materials

Sodium hydroxide (NaOH, Aldrich, >97%) was used for the retting of kenaf ribbon after it was dissolved in deionized water (W, resistivity of 18 MΩ cm via Milli-Q Advantage System). Potassium hydroxide (KOH, Sigma-Aldrich, 90%) and hydrochloric acid (HCl, Sigma-Aldrich, 37%) were purchased and used without further purification. Cellulose acetate filter (Advantech, USA) along with CR2032 coin cell was utilized for the preparation of full symmetric cells for the electrochemical study.

Preparation of activated carbon monolith of kenaf (ACMK)

The ACMK was prepared from the kenaf fibers obtained from local-farm-grown kenaf plant by soaking it in distilled water for ~24 h and separating the bast ribbon. The ribbons were then subjected to retting in 2% NaOH aqueous solution for 1 h at 90 °C and neutralized with acetic acid.[25] Next, they were rubbed to obtain the fibers which were dried at RT for 48 h and then 12 h at 80 °C. Finally, the kenaf fibers were powdered, sieved (20 mesh) and then stored in a desiccator until use. The resulting powder (4 g) was placed in a steel mould (diameter of ~16 mm) and pressed at 10 klb to form column-shape samples.

The prepared monoliths were subjected to pyrolysis in a tube furnace (MSTF-1100, Myungsung Eng., Korea) at 500, 600, 700

or 800 °C for 4 h at a heating rate of 5 °C min^{-1} under the N_2 flow of 200 sccm. Then, the carbon monolith of kenaf (CMK) was machined to a diameter of ~10 mm, cut into ~1 mm thick disc samples and immersed in 6 M KOH aqueous solution overnight under reduced pressure. After drying at RT and then 90 °C, the weight gain was measured to attain a better understanding of the activation behaviour. The samples were activated in a tube furnace at 700 °C for 1 h at a heating rate of 5 °C min^{-1} under the N_2 flow of 200 sccm to generate activated CMK (ACMK). The ACMK was immersed in 1 M HCl solution overnight to remove the residual K and washed copiously, followed by grinding with sand paper to achieve a weight of ~10 mg. The samples were named ACMK-xxx where xxx represents the pyrolysis temperature (PYT) of 500, 600, 700 or 800 °C, while CMK-xxx represents corresponding samples without activation. For comparison, the CMK was subjected to heat treatment at 700 °C for 1 h and named HCMK (heat treated CMK).

Characterization of activated carbon monolith of kenaf (ACMK)

FE-SEM (Gemini-500, Zeiss, Germany) was utilized at 10 keV for the ACMK, CMK and as-moulded monoliths of kenaf with carbon coating, while ACMK-500 was studied with FE-TEM (JEM-2100F, Jeol, Japan). The ACMK and CMK were also studied by Raman spectroscopy (UniRam-5000, UniThink, Korea, JASCO NRS-5100) equipped with 532 nm laser. In addition, XRD (Empyrean, X'Pert PRO Multi-Purpose) with a Cu target, as well as XPS (Thermo Scientific, K-Alpha$^+$, USA) with a monochromatized Al Kα source (1486.6 eV) were also used for the characterization of ACMK. The latter provided survey scan and the narrow scans of C_{1s} and O_{1s} peaks. The C_{1s} peak was subjected to deconvolution to gain a better understanding of the oxygen functional moieties. Pore characteristics of ACMK as well as CMK were studied with an adsorption instrument (ASAP-2010, Micromeritics, USA) using N_2 at −196 °C. The specific surface area (SSA) and the pore size distribution were calculated by Brunauer–Emmett–Teller (BET) method and non-local density functional theory (NLDFT) respectively, while the mean pore diameter was obtained from 4 V/SSA. The total pore volumes were calculated from the total single point adsorption of pores with a radius less than 300 nm at $P/P_0 = 0.99$, while micro-pore volumes were obtained via the t-plot theory. TGA (PerkinElmer TGA-4000, USA) was also performed on ACMK, HCMK and CMK samples at 10 °C min^{-1} under the N_2 flow of 20 cc min^{-1}.

Electrochemical property measurement

Electrochemical properties of ACMK were studied with 6 M KOH electrolytes using Versa STAT 3 Instrument (Princeton Applied Research, USA) via a three-electrode system first. The disc-shape ACMK (approximately 10 mm in diameter, 10 mg in weight) was utilized as the working electrode, and a platinum gauze (1 × 1 cm) and Ag/AgCl (saturated KCl) were used as the counter and reference electrodes, respectively. The CV was carried out in the −1–0 V range at a scan rate of 2–100 mV s^{-1},

while the GCD was performed at a current density of 1–20 A g^{-1}. The electrochemical impedance spectroscopy (EIS) was also recorded in the 0.01–100 kHz range with an amplitude of 10 mV. The specific capacitance (C_{sp}) was calculated from the GCD study based on the formula of $C_{sp} = (I \times t)/(\Delta V \times m)$,[26] where I is the charge–discharge current, t is the time of discharge, ΔV is the discharge voltage difference between the discharge time, and m is the mass of the active material.

The sample for the two-electrode system was prepared with a CR2032 coin cell, cellulose acetate filter (Advantech, USA) and two ACMK discs (approximately 10 mm in diameter and 10 mg in weight) that exhibited the highest C_{sp} in the three-electrode system. The same conditions as the three-electrode system were utilized for the GCD in 6 M KOH aqueous solution. The C_{sp} was calculated, along with energy and power densities, using the formula reported already.[27] The cycling stability of ACMK was also evaluated up to 5000 cycles of the charging–discharging process at a current density of 1 A g^{-1}.

Results and discussion

Preparation of activated carbon monolith of kenaf (ACMK)

The column-shape carbon monolith of kenaf (CMK) was successfully prepared by moulding the kenaf fibers and carrying out pyrolysis at 500, 600, 700 or 800 °C for 1 h (Fig. S1†). The CMK maintained its shape upon pyrolysis, but exhibited large weight losses of 74.7, 77.3, 79.5 and 80.7% for CMK-500, CMK-600, CMK-700 and CMK-800, respectively (Table S1†). These losses are comparable to 83.7% weight loss reported at 700 °C pyrolysis of the kenaf fiber.[28] As expected, the weight loss increased slightly with higher PYT, indicating increased carbonization, as reported earlier,[28] but it is not clear whether 800 °C was high enough to give complete pyrolysis. The diameter shrinkage measured was 17.5, 20.5, 22.9 and 23.2% for CMK-500, CMK-600, CMK-700 and CMK-800, respectively (Table S1†) and increased with higher PYT, as expected.

Upon KOH impregnation of the 1 mm thick disc-shape samples, weight gains of 55.1, 53.7, 54.3 and 53.5% were observed for CMK-500, CMK-600, CMK-700 and CMK-800, respectively (Table S1†). It is noted that the gains are similar to each other, which can be explained by the very similar SEM micrographs of CMKs regardless of the PYT (will be discussed later).

Activation at 700 °C for 1 h resulted in the weight loss of 18.7, 13.9, 9.3 and 7.8% for ACMK-500, ACMK-600, ACMK-700 and

ACMK-800, respectively (Table S1†). The weight loss decreased with higher PYT despite the similar KOH gains regardless of the PYT, as previously reported with resorcinol–formaldehyde.[10] This trend can be explained by the 2nd pyrolysis taking place during activation as a result of the incomplete carbonization which was evidenced by the increased weight remains with lower PYT upon pyrolysis (Table S1†). This was possible because of the two-step process (pyrolysis and then activation) taking place in this study.

Consequently, in order to demonstrate that a 2nd pyrolysis occurred during activation, the CMKs were heat treated at 700 °C for 1 h, which was the same condition used for activation with the exception of KOH impregnation. This provided a weight loss of 13.3, 7.7, 4.9 and 3.5% for HCMK-500, HCMK-600, HCMK-700 and HCMK-800, respectively (Table S1†), proving that the 2nd pyrolysis occurred since carbonization remained incomplete after the first pyrolysis step. It is noted that these losses are slightly smaller than the ones from activation (18.7, 13.9, 9.3 and 7.8%), showing a difference of ~5% which can be attributed to the weight loss from true KOH activation.

It is also interesting to note that the colour of KOH solution turned brown upon immersion of the ACMK, and that a stronger colour was observed with the ACMK from lower PYT. This can be ascribed to the dissolution of components in the ACMK because of the incomplete carbonization that took place after pyrolysis and activation. A similar trend was also observed from the HCMK, which will be correlated to the TGA results in the following section.

The TGA analysis of CMKs under N$_2$ flow at 10 °C min^{-1} showed a slow weight loss with clear PYT dependence, providing 11.7, 7.2, 5.2 and 4.1% at 700 °C for CMK-500, CMK-600, CMK-700 and CKM-800, respectively (Fig. 1a). As expected, a higher weight loss was obtained with lower PYT, since incomplete carbonization increased with lower PYT (Table S1†), thus, resulting in increased 2nd pyrolysis. Interestingly, similar weight losses were obtained from the TGA as well as the heat treatment (13.3, 7.7, 3.9 and 3.5%). It can be said that the heat treatment at 700 °C had a similar effect as the TGA study carried out to 700 °C. The 2nd TGA of CMKs exhibited a slow weight loss with clear PYT dependence (Fig. S2a†), which is related to the incomplete carbonization even after the 1st TGA. However, no PYT dependence was observed from the 3rd TGA (Fig. S2b†), suggesting that complete carbonization has occurred during
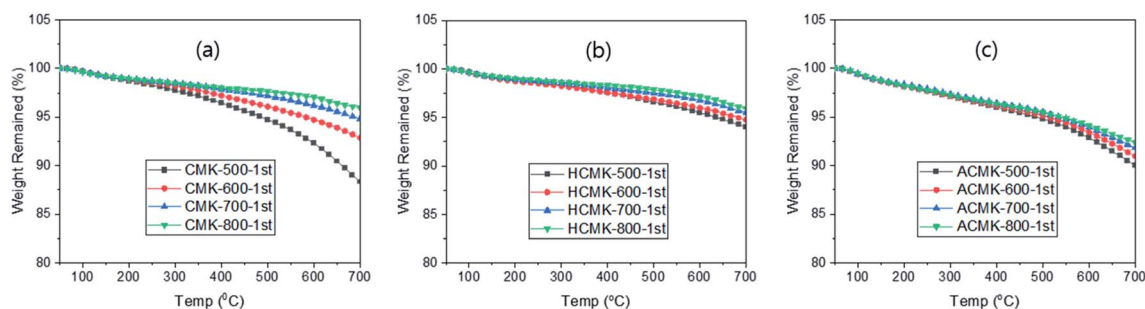

Fig. 1 The 1st TGA of CMK (a), HCMK (b) and ACMK (c) under N$_2$ flow of 20 cc min^{-1}.
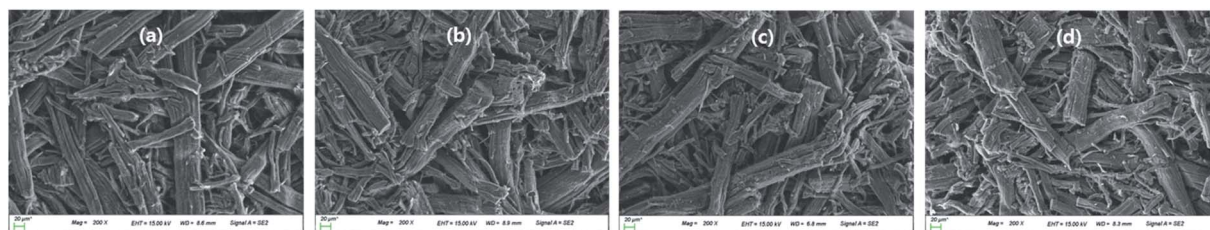
Fig. 2 SEM micrographs of ACMK-500 (a), ACMK-600 (b), ACMK-700 (c) and ACMK-800 (d).

the 2nd TGA and that the weight loss in the 3rd TGA is due to thermal degradation.[29]

As expected from the heat treatment at 700 °C prior to the TGA, the 1st TGA of HCMKs exhibited much lower weight loss than the 1st TGA of CMKs (Fig. 1b), as a result of the 2nd pyrolysis upon heat treatment. But these losses are similar to those from the 2nd TGA of CMKs, possibly owing to the similar effect of the heat treatment and the 1st TGA for CMKs, both of which resulted in the 2nd pyrolysis. As noted, the 1st TGA of HCMKs exhibited PYT dependence, similar to the 2nd TGA of CMKs, which can be attributed to the incomplete carbonization despite the 2nd pyrolysis that occurred *via* the heat treatment. This can also be related to the colour change of the HCMKs upon their immersion in the KOH aqueous solution, as discussed above. However, no PYT dependence was observed in the 2nd TGA of HCMKs, indicating complete carbonization *via* the 1st TGA of HCMKs (Fig. S2c†).

These can be compared with the results of ACMKs, which exhibited larger weight losses than the HCMKs in the 1st TGA scan (Fig. 1c). This is likely due to the loss of the functional moieties which were introduced by activation[30] as well as to the 2nd pyrolysis, as observed with HCMKs. The latter can be related to the colour change of KOH solution after the immersion of ACMKs. The 2nd TGA of ACMKs exhibited similar weight losses regardless of the PYT (Fig. S2d†) as the HCMKs, as a result of complete removal of the functional moieties and complete carbonization *via* the 1st TGA.

In the SEM analysis, the as-moulded column-shape samples showed kenaf fibers with a wide range of diameters (20–80 μm) and some small debris on the fiber surface, along with a dent-like deformation on some fibers (Fig. S3†) which likely arises from the high pressure (10 klb) used for moulding. Upon pyrolysis at 500 °C, the maximum diameter of the fiber

decreased to ~60 μm, and the fiber surface became cleaner and smoother despite some small particles still remaining on the fibers (Fig. S4a†) and line-shape defects along the fiber direction.[31] Similar micrographs were obtained from CMK-600, CMK-700 and CMK-800 (Fig. S4†), as expected from the small difference in the weight loss upon pyrolysis regardless of the PYT (Table S1†).

Pores were also observed in the cross-section of some fibers (Fig. S5†), as reported previously,[28] but no pores were present on the surface of the fiber. Upon KOH activation, a clean surface without any debris was observed, but the line-shape defects along the fiber direction became clear (Fig. 2), which is related to the further weight loss upon activation, and thus, possible deeper defects (Table S1†). It is noted that all SEM micrographs appeared similar regardless of the PYT, which is attributed to the similar KOH gain, and thus, similar degree of activation, as discussed above. For comparison, ACMK-500 was analysed by TEM.

The XRD spectra of ACMKs showed broad peaks around 23° and 43°, as reported earlier,[16,32] corresponding to (002) and (100) from turbostratic or disordered graphite,[33] as shown in Fig. 3a. The (002) peak shifted slightly to a higher diffraction angle with higher PYT, likely due to the increased ordering.[34] Raman characterization of the ACMKs was also carried out, as shown in Fig. 3b, and showed two peaks at ~1370 and ~1590 cm^{-1}, as expected,[16,18] These peaks can be attributed to the D-bands from the breathing mode of the sp^2 carbons on the edges or defects, as well as to the G-bands from the stretching motion of the sp^2 carbons, as reported previously.[35] The intensity ratio of these peaks (I_D/I_G), which is known to be related to the degree of disorder, was calculated to be 1.62, 1.54, 1.45, and 1.39 for ACMK-500, ACMK-600, ACMK-700 and ACMK-800, respectively. This decrease can be related to the increased ordering with
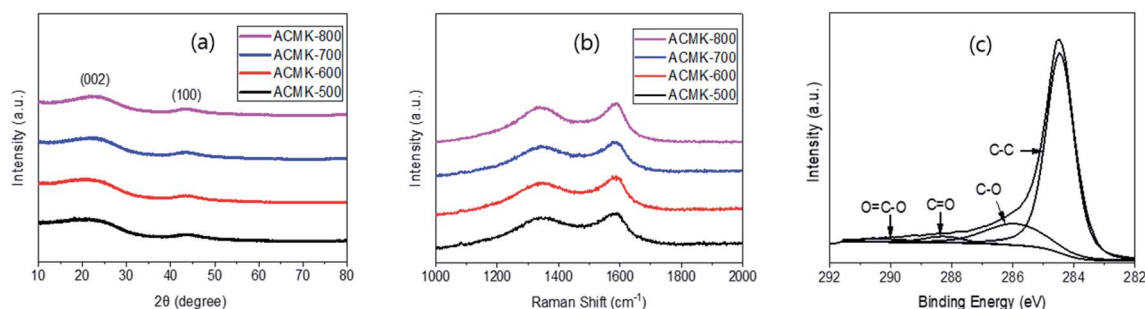

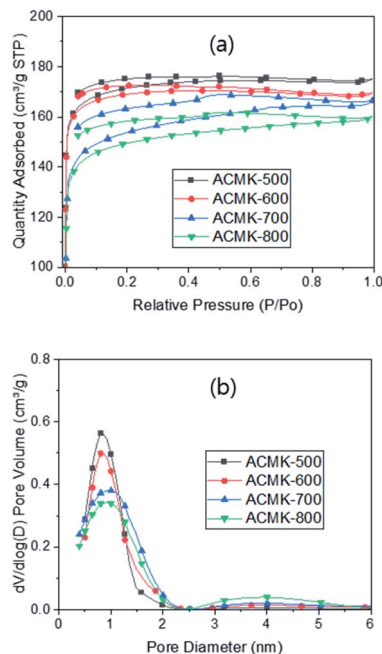**Fig. 3** XRD (a) and Raman (b) of ACMK as well as (c) C$_{1s}$ peak of ACMK-500.

Fig. 4 N_2 sorption (a) and pore size distribution (b) of ACMKs.

higher PYT, as reported previously,[36] which is also supported by the peak shift observed in the XRD results in Fig. 3a.

It is interesting to note that these I_D/I_G ratios are similar to those from the CMKs, showing 1.67, 1.53, 1.45, and 1.35 for CMK-500, CMK-600, CMK-700 and CMK-800, respectively (Fig. S6a†). However, this trend is different from those in the literature, which reported higher I_D/I_G ratios upon activation.[37] The similar I_D/I_G ratios for CMKs and ACMKs can be explained by the increased I_D/I_G ratio resulting from activation, which was then nullified by the decreased I_D/I_G ratio *via* the 2nd pyrolysis, as reported previously.[10] This was possible because of the low loading (~50%) of KOH for activation in this study, leading to a small increase in the I_D/I_G ratio, compared with the high loading of KOH such as ~400% used in the literature[37] that resulted in a greatly increased I_D/I_G ratio. Thus, the I_D/I_G ratios of HCMKs were evaluated in order to understand this behavior, which provided 1.43, 1.37, 1.31 and 1.24 for HCMK-500, HCMK-600, HCMK-700 and HCMK-800, respectively (Fig. S6b†). One can see a small decrease in the I_D/I_G ratio upon the heat treatment due to the increased ordering arising from the 2nd pyrolysis. Thus, the lack of change in the I_D/I_G ratio observed upon activation can be explained by a small increase in the I_D/I_G ratio

upon activation, which was possible because of the low loading of KOH.

In the XPS analysis, ACMKs exhibited C_{1s} and O_{1s} peaks at around 285 and 532 eV in the wide scan, respectively, while atomic concentration of the C_{1s} increased slightly with higher PYT, showing 90.6, 91.7, 92.5 and 93.9% for ACMK-500, ACMK-600, ACMK-700 and ACMK-800, respectively. This increase can be related to the higher degree of pyrolysis with higher PYT, as evidenced by the higher weight loss with higher PYT in the pyrolysis (Table S1†). As expected, almost identical C_{1s} peaks were observed regardless of the PYT (Fig. S7†), possibly due to the similar gains of KOH, and thus, similar degrees of activation regardless of the PYT. Deconvolution of the C_{1s} peak of ACMK-500 provided strong C–C and relatively weak C–O, C=O and O–C=O peaks at 284.6, 286.1, 288.3 and 290.2 eV, respectively (Fig. 3c), similar to those reported in the literature.[31]

The pore characteristics of ACMKs were studied *via* the N_2 sorption measurement and exhibited a Type I isotherm with H4 hysteresis (Fig. 4a), similar to the one reported earlier.[18,31] Such hysteresis can be attributed to the slit-shape mesopores.[38] The hysteresis became larger with higher PYT, which is related to the deeper slit-shape meso-pores with higher PYT. This is supported by the clear line-shape defects observed in the SEM micrographs. The N_2 adsorption decreased with higher PYT, providing a specific surface area (SSA) of 693, 667, 641 and 602 $m^2 \, g^{-1}$ for ACMK-500, ACMK-600, ACMK-700 and ACMK-800, respectively (Table 1).

A similar trend was observed in the studies with RF-based[10] as well as chitosan-based[39] activated carbons, but most studies in the literature reported an opposite trend of increasing SSA with higher activation temperature,[40] unless the activation temperature was so high that it led to pore collapsing.[41] The different trend can be explained by the two-step process used in this study, pyrolysis followed by activation, compared with the one-step process (simultaneous pyrolysis and activation) employed in those studies. The pyrolysis (1st step) in this study resulted in incomplete carbonization, as discussed above (Table S1†), which induced the 2nd pyrolysis during activation (2nd step), as demonstrated by TGA studies. This resulted in extra weight loss, in addition to the loss from activation, leading to extra pore generation and increased SSA. The extra pore generation increased with lower PYT because of the increased incomplete carbonization, thus, increasing the 2nd pyrolysis with lower PYT, as discussed above (Table S1†). However, there would be no chance for the 2nd pyrolysis to occur in the one-step process since pyrolysis and activation take place simultaneously, which in turn means no extra pore generation.

Table 1 Pore characteristics of ACMK *via* N_2 sorption study

	S^a ($m^2 \, g^{-1}$)	V_{total}^b ($cm^3 \, g^{-1}$)	V_{micro}^c ($cm^3 \, g^{-1}$)	MPD^d (nm)
ACMK-500	693	0.271	0.261 (96.3%)	1.314
ACMK-600	667	0.269	0.258 (95.9%)	1.328
ACMK-700	641	0.265	0.247 (93.2%)	1.343
ACMK-800	602	0.253	0.233 (92.1%)	1.346

[a] Specific surface area. [b] Total pore volume. [c] Micro pore volume. [d] Mean pore diameter.

The SSA of 693–602 m^2 g^{-1} from ACMKs in this study can be compared with 3–5 m^2 g^{-1} from CMKs, demonstrating greatly increased SSA *via* the activation as well as the 2nd pyrolysis, while the latter is similar to 3–29 (ref. 42) and 13 m^2 g^{-1} (ref. 43) in the literature. The SSA of 693 m^2 g^{-1} from ACMK-500 in this study can be compared with 1742,[44] 1570,[32] 1154,[21] and 1031,[42] 493,[20] 330,[19] 289,[45] and 285 m^2 g^{-1} (ref. 46) from the kenaf-based carbons. It can be seen that a wide range of SSA has been reported, depending on the pyrolysis and/or activation conditions and the activating agents used. Unfortunately, no capacitance data were available to be correlated to these SSAs. The pore size analysis showed the presence of micro- as well as meso-pores (Fig. 4b). As expected, the highest micro-pore volume (percentage) was obtained from ACMK-500 (Table 1). This can be attributed to the highest degree of the 2nd pyrolysis which generated more micro-pores than others. This can also be related to the smallest average pore size of ACMK-500 and the increased slit-shape meso-pores obtained with higher PYT, as supported by the increased hysteresis.

Electrochemical characterization of activated carbon monolith of kenaf (ACMK)

The cyclic voltammetry (CV) curves of ACMKs were obtained with a three-electrode system at the scan rate of 2 mV s^{-1} in the −1 to 0 V range (Fig. 5a). The curves were rectangular in shape regardless of the PYT, indicating that the ACMKs exhibit ideal capacitive characteristics. The largest curve size was obtained from ACMK-500, followed by ACMK-600, ACMK-700 and ACMK-800, as expected from the decreased SSA with higher PYT. Since ACMK-500 had the largest CV curve, it was subjected to a scan rate variation from 2 to 100 mV s^{-1}. The results showed a change in the curve shape from rectangular to quasi rectangular (Fig. S9†), as reported elsewhere.[47] A wide hump was observed in the range of −0.9 to −0.4 V (Fig. 5a), indicating the existence of pseudocapacitance[48] likely arising from the functional moieties on the electrode surface, which was supported by the XPS results (Fig. 3c). The size of the pseudocapacitance peak decreased slightly with higher PYT, corresponding to the decreased oxygen concentration.

Galvanostatic charge–discharge (GCD) was also performed since it is known to be an efficient way to measure the specific capacitance of activated carbons. The GCD curves of ACMKs showed a typical isosceles triangular-shape and their discharge time decreased with higher PYT (Fig. 5b), as expected from the CV curves. A small IR drop was also observed, indicating a small internal resistance, which decreased with higher PYT, likely due to the increased ordering, as evidenced by the XRD and Raman results. Based on these GCD curves, the specific capacitance (C_{sp}) was calculated to be 217, 191, 180 and 164 F g^{-1} for ACMK-500, ACMK-600, ACMK-700 and ACMK-800, respectively. The decreasing capacitance can be related to the decreased SSA with higher PYT. As discussed above, ACMK-500, which had the largest SSA, provided the highest C_{sp}. Thus, it can be said that the two-step process is more advantageous than the one-step process in obtaining a high C_{sp} despite the extra cost. In this regard, the pyrolysis temperature has to be low enough to induce a high degree of extra pore generation *via* the 2nd pyrolysis, but high enough to achieve good mechanical stability for the electrode.

The highest C_{sp} of 217 F g^{-1} obtained in this study is much higher than 37 F g^{-1} from the kenaf-fiber-based AC and 136 F g^{-1} from aniline coating.[16] But it is lower than 416 F g^{-1} from the kenaf stem-based AC with MnO$_2$ coating[17] or 327 F g^{-1} from the NiCl$_2$ activated nanosheet of kenaf stem.[18] The latter two studies suggest that the capacitance in this study can possibly be increased by coating of pseudocapacitive materials
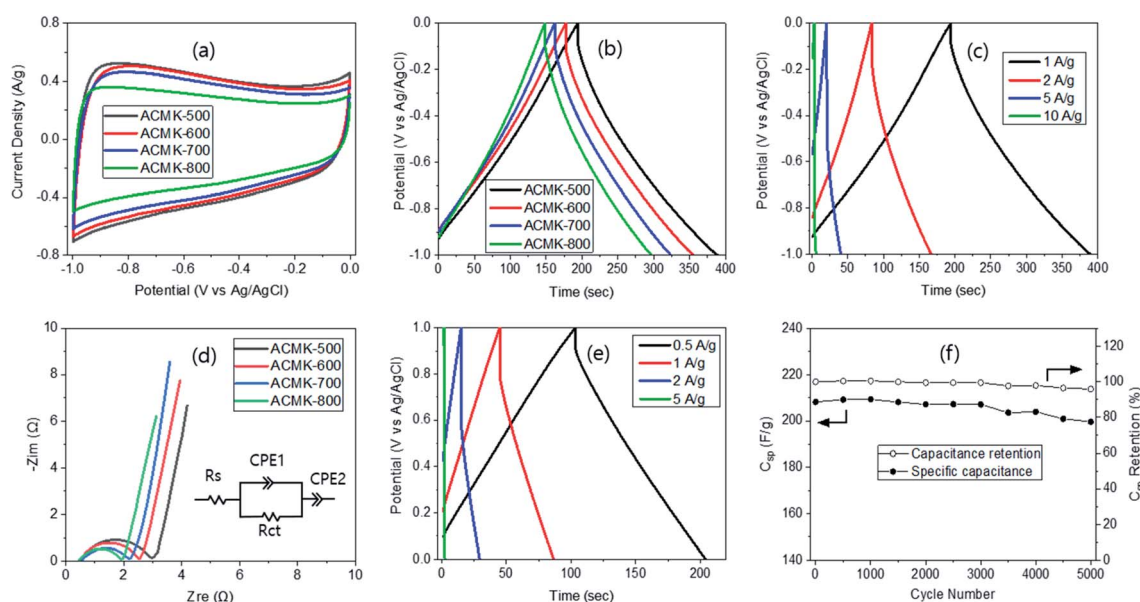

Fig. 5 CV (a), GCD (b and c) and Nyquist plot (d) of ACMK *via* a three-electrode system as well as GCD (e) and cycling test (f) of ACMK-500 *via* a two-electrode system.

Paper

RSC Advances

or by a special type of activation. Higher C_{sp} of 405, 367, 345, 298, and 268 F g^{-1} have also been reported from the bean curd stick byproduct,[49] chitonsan,[39] jujube pit,[50] lotus leaf[51] and coconut shell,[52] respectively. Of course, there are also a number of studies, reporting smaller specific capacitance as well. Since ACMK-500 exhibited the highest C_{sp}, it was subjected to current density variation, as shown in Fig. 5c. As expected, the isosceles triangular-shape GCD curves were observed, but an increased IR drop and a decreased charge–discharge time were displayed with higher current density. Based on these, the C_{sp} was calculated to be 217, 205, 196 and 162 F g^{-1} at 1, 2, 5, and 10 A g^{-1}, respectively, resulting in 75% retention at 10 A g^{-1}.

Electrochemical impedance spectroscopy (EIS) of ACMKs was also carried out in order to elucidate the diffusion kinetics of the electrolyte ions in the samples and their corresponding Nyquist curves are shown in Fig. 5d. The equivalent serial internal resistances (R_s) of ∼0.5 Ω was calculated from all samples, which is attributed to the small resistance of ACMK due to the functional moieties generated from activation and their high affinity to electrolytes.[53] The charge transfer resistance (R_{ct}) was also calculated, providing 2.4, 2.1, 1.7 and 1.4 Ω for ACMK-500, ACMK-600, ACMK-700 and ACMK-800, respectively. The R_{ct} decreased with higher PYT as a result of increased ordering with higher PYT, which is supported by the XRD and Raman results. The very small Warburg impedance and almost vertical line in the low-frequency range can be related large pore structure, as demonstrated by SEM (Fig. S5†) as well as TEM micrograph (Fig. S8†). The equivalent circuit model fot ACMK-500 was obtained with ZSimpWin software, as shown in Fig. 5d.

For comparison, a two-electrode system was also studied via GCD at the current density ranging from 0.5 to 5 A g^{-1}. As expected, an isosceles triangular-shape was obtained with a nearly linear charge–discharge slope (Fig. 5e), demonstrating an excellent electrochemical double-layer behaviour. In addition, the charge–discharge time was also about half of that for the three-electrode system, which is similar to the results reported earlier,[27] possibly due to the doubled weight of the electrode. Based on these GCD curves, the C_{sp} was calculated to be 212, 197, 183 and 171 F g^{-1} at 0.5, 1, 2 and 5 A g^{-1}, respectively. These values were slightly lower than those from the three-electrode system at a given current density. The energy and power densities were calculated to be 6.0 W h kg^{-1} and 215 W kg^{-1}, respectively, using the formula reported earlier.[26] These values can be compared with the energy density of 16–12.3 W h kg^{-1} at the power density of 200–10 068 W kg^{-1} for NiCl$_2$ activated kenaf fibers (416F g^{-1})[18] or 17.3–6.9 W h kg^{-1} at the power density of 198–3175 W kg^{-1} for the MnO$_2$ coated kenaf,[17] 8.95 W h kg^{-1} at the power density of 250 W kg^{-1} for jujube[50] and 9.2 W h kg^{-1} at the power density of 490 W kg^{-1} (ref. 51) for lotus leaves.

The cycling stability of ACMK-500 was also evaluated at 1 A g^{-1} (Fig. 5f) and showed high cycling stability with 95.9% remains in capacitance after 5000 cycles of the charging-discharging process. This can be compared with 95.6% from 5000 cycles[18] and 86% from 1000 cycles.[17] However, it is slightly lower than 100% obtained from the RF-based carbon[10] and may result from the small pore size with an absence of inter-connectivity of pores. The results in this study demonstrate that

ACXM-500 is a promising electrode material for electrochemical supercapacitors, while its energy and power densities can be possibly enhanced by a coating of pseudocapacitive materials.

Conclusions

Activated carbon monoliths of kenaf (ACMKs) were successfully prepared from kenaf fibers by moulding column-shape samples and subjecting them to pyrolysis and activation. N$_2$ adsorption of ACMKs exhibited increased SSA with lower PYT, which is attributed to the increased incomplete carbonization upon pyrolysis, which in turn resulted in extra pore generation via a 2nd pyrolysis during activation. The CV study with a three-electrode system provided rectangular-shape curves, indicating an ideal capacitive behaviour of ACMKs, while the decreased curve size with higher PYT can be related to the decreased SSA. A small hump observed in the −0.9−−0.4 V range is an indication of pseudocapacitance arising from the oxygen functional moieties, as evidenced by the XPS study. The GCD study showed isosceles triangular curves and decreased charge–discharge time with higher PYT. The C_{sp} from the GCD curves decreased with higher PYT, showing 217, 195, 180 and 165 F g^{-1} for ACMK-500, ACMK-600, ACMK-700 and ACMK-800, respectively. This is related to the decreased SSA with higher PYT. When the current density was varied, ACMK-500 exhibited C_{sp} of 217, 202, 192, 162 F g^{-1} at 1, 2, 5 and 10 A g^{-1}, respectively. The EIS study exhibited a small semicircle at high frequency as well as a 45-degree inclined line in the mid- and low-frequency range, demonstrating the slow diffusion of the electrolytes, which can be attributed to the slit-shape meso-pores. The two-electrode system with ACMK-500 provided isosceles triangular curves in the GCD measurement, providing C_{sp} of 212, 197, 183 and 171 F g^{-1} at 0.5, 1, 2 and 5 A g^{-1}, respectively. The energy and power densities were also calculated to be 6.0 W h kg^{-1} and 215 W kg^{-1}, respectively. The cycling stability at 1 A g^{-1} showed 95.9% remain in capacitance after 5000 cycles. These results demonstrate that ACMK-500 is a promising electrode material for high-performance electrochemical supercapacitors.

Conflicts of interest

There are no conflicts to declare.

Acknowledgements

Notes and references

1 K. Koehlert, *Chem. Eng.*, 2017, 32.
2 R. Dubey and V. Guruciah, *Ionics*, 2019, **25**, 1419.
3 R. W. Pekala, *J. Mater. Sci.*, 1989, **24**, 3221.
4 A. Feinle, M. S. Elsaeser and N. Huesing, *Chem. Soc. Rev.*, 2016, **45**, 3377.